

ChemComm

Accepted Manuscript



This is an *Accepted Manuscript*, which has been through the Royal Society of Chemistry peer review process and has been accepted for publication.

Accepted Manuscripts are published online shortly after acceptance, before technical editing, formatting and proof reading. Using this free service, authors can make their results available to the community, in citable form, before we publish the edited article. We will replace this *Accepted Manuscript* with the edited and formatted *Advance Article* as soon as it is available.

You can find more information about *Accepted Manuscripts* in the [Information for Authors](#).

Please note that technical editing may introduce minor changes to the text and/or graphics, which may alter content. The journal's standard [Terms & Conditions](#) and the [Ethical guidelines](#) still apply. In no event shall the Royal Society of Chemistry be held responsible for any errors or omissions in this *Accepted Manuscript* or any consequences arising from the use of any information it contains.

COMMUNICATION

p-Doped Three-Dimensional Graphene Nano-Networks Superior to Platinum as a Counter Electrode for Dye-Sensitized Solar Cells

Cite this: DOI: 10.1039/x0xx00000x

Received 00th January 2012,
Accepted 00th January 2012

Hyo-Jin Ahn, Ik-Hee Kim, Jong-Chul Yoon, Sun-I Kim, and Ji-Hyun Jang*

DOI: 10.1039/x0xx00000x

We report CVD-grown p-doped three-dimensional graphene nano-networks (3D-GNs) that provide superior performance to Pt as a counter electrode material in dye sensitized solar cells (DSSCs). The 3D-GN based DSSC exhibits a maximum photoconversion efficiency of 8.46%, which is 6.01% greater than that obtained from Pt based DSSCs.

A dye-sensitized solar cell (DSSC) is a low cost photovoltaic system that converts solar energy directly into electrical energy with high energy conversion efficiency.^{1,2} The DSSC is one of the most promising candidates for alternative renewable energy devices due to its inexpensive and highly scalable process. A typical DSSC consists of dye, an electrolyte containing redox couples, a wide bandgap nanocrystalline TiO₂ as a working electrode, and a counter electrode. In general, cost-inefficient Pt has been necessarily used as the standard counter electrode material in DSSCs due to its high stability, good conductivity, and outstanding electrochemical activity. Thus, finding good counter electrode materials with superior performance to Pt is urgent and critical for the realization of low-cost DSSCs. In light of this, graphene, which is analogous to carbon materials yet with many superior properties, has potential as a novel material for the counter electrode in DSSCs.³⁻⁵

Graphene is a two-dimensional material with a one-atom-thick layer of sp²-bonded carbon atoms in a honeycomb lattice with excellent electrical conductivity and large theoretical specific surface area.⁶⁻⁸ The authors recently reported bi-continuous three-dimensional graphene nano-networks (3D-GNs) with controlled dimensions prepared via precursor-assisted CVD in a bulk scale with outstanding electrical conductivity and large surface area.⁹ The 3D-GNs fabricated by this method have much larger surface area than 3D graphene foam fabricated via a nickel frame with a few hundred micrometer scale.¹⁰ They are also substantially superior to reduced graphene paper fabricated by vacuum filtration of chemically modified graphene in terms of conductivity.¹⁰⁻¹² We hypothesize that these two important properties can be effectively exploited to improve the performance of a state-of-the-art Pt substitutable counter electrode (CE) in DSSCs. Furthermore, this technique utilizes nontoxic iron as a catalyst for CVD growth of graphene, the fourth most common element in the earth's crust, which will broaden the applicability of graphene in terms of fabrication cost and environmental safety of DSSCs. Here, we report p-doped precursor-assisted CVD grown 3D-GNs with a conductivity of 7 S/cm and a surface area of 1,025 m²/g as an excellent single component CE material that outperforms to Pt. An optimized 3D-GN-based DSSC

shows 6.01% higher power conversion efficiency than a Pt-based DSSC, and provides a direct route to mass-producible and cost-efficient DSSCs by replacing Pt.

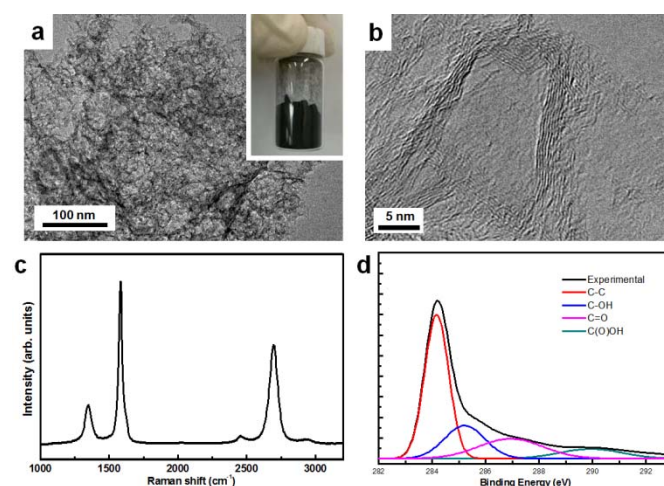


Figure 1. a) Large area TEM image of 3D-GNs. The inset reflects gram scale synthesis of CVD-grown 3D-GNs. b) Close-up TEM image of single ball of graphene. c) Raman spectrum of 3D-GNs. d) XPS spectrum of C1s in 3D-GNs.

Taking into consideration that oxygen-containing functional groups in carbon materials are responsible for the electrocatalytic performance of CE in DSSCs,^{13, 14} the Pt alternatives targeted here are bulk scale precursor-assisted CVD grown 3D-GNs with a slightly detectable degree of defects (oxygen atoms) while retaining good conductivity. The experimental details for 3D-GNs are found in supporting information. Figure 1a shows transmission electron microscope (TEM) images of low-density 3D-GNs near the edges, clearly showing nano-cavities of the 3D-GNs. The digital camera image of gram scale 3D-GNs in the inset confirms the mass-production capability of precursor-assisted CVD-grown 3D-GNs. The close-up TEM image in Figure 1b shows a single unit cell of few-layer graphene ball with a diameter of ~30 nm. Figure 1c is the Raman spectrum of a 3D-GN fabricated via drop casting of an iron precursor solution followed by the CVD growth of graphene. The maximum ratio of I_D/I_G and the minimum ratio of I_D/I_G are 1.28 and 0.23, respectively, indicating reasonable quality of 3D graphene networks. Figure 1d shows the C1s XPS spectrum of 3D-GNs with

an intense and strong peak at 284.2 eV, originating from C-C and C=C, with a relatively small portion of defect peaks at 285.5 eV, 287.4 eV, and 289.3 eV, in good agreement with the Raman spectrum. The average conductivity of the pristine 3D-GN powders was 5 S/cm (Figures S2-S3), which is comparable to the previously reported value of 10 S/cm of graphene foam created from a micron-scale nickel nanoframe.¹⁰ The surface area of the 3D-GNs obtained by BET measurement was a surprisingly high value of 1,025 m²/g with pore size of 13 nm (Figure S4).⁹

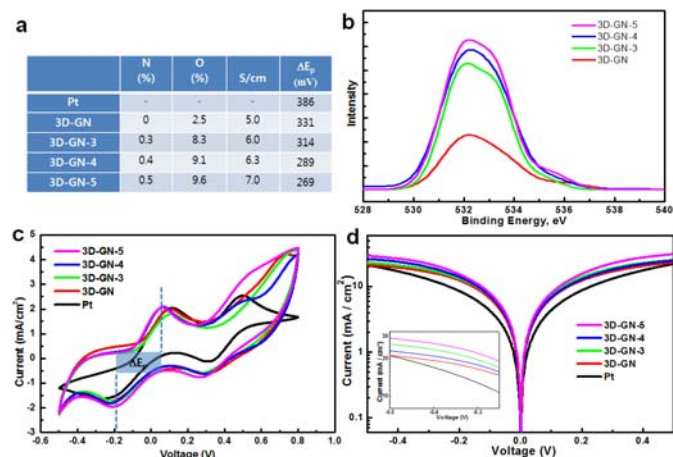


Figure 2. Comparison of p-doped 3D-GNs with various contents of N and O atoms. a) Summary of physical properties of the samples. b) XPS spectrum of O1s of 3D-GNs. c) Cyclic voltammograms of iodide species in DSSC cells at a scan rate of 50 mV/s. d) Tafel curves of symmetric dummy cells.

It has been reported that the properties of graphene can be tailored by the incorporation of other functional groups onto the matrix of graphene. For instance, enhanced electrical conductivity of graphene is attainable by deposition of dopant atoms on the graphene lattice^{4, 15} and an optimum catalytic effect of graphite in DSSCs can be achieved by the addition of a small amount of oxygen-containing functional groups on the surface of graphene.^{13, 14} Here we report that CVD-grown pristine 3D-GNs can be optimized as a CE in DSSCs by simple doping of heteroatoms. By slightly increasing the content of nitrogen and oxygen via a p-doping process of 3D-GNs, both the conductivity and catalytic activity were noticeably improved. Figure 2 compares the electrochemical activity of p-doped 3D-GNs with various contents of N and O atoms by immersing 3D-GNs in HNO₃ solutions with various concentrations. The chemical compositions of p-doped graphene obtained by an elemental analysis are listed in Figure 2a with the values of conductivity. The fractional amounts of N atoms in 3D-GNs immersed in HNO₃ solutions of 50, 75, and 100 wt% for 30 min were measured to be 0.3, 0.4, and 0.5 wt% and the corresponding samples are denoted as 3D-GN-3, 3D-GN-4, and 3D-GN-5, respectively. The measured conductivity of p-doped 3D-GNs reveals a linear relationship with the content of N atoms and is enhanced up to 7 S/cm. A further increase of immersion time did not improve the conductivity of the samples. Figure 2b shows the XPS spectra of O1s, the peak at the 531.8 eV region, increasing with increasing the concentration of HNO₃ solutions, indicating a greater degree of incorporation of O atoms which beneficially impact electrocatalytic performance. It should be noted that the conductivity, which can be adversely affected by a large amount of oxygen content, was not deteriorated up to this point, due to the increase of the nitrogen content (Figure 2a).¹⁵ Our approach is different from other methods aimed at enhancing the conductivity of

chemically prepared graphene in that we first ensured sufficient conductivity of graphene via the CVD growth process and further enhanced both the conductivity and catalytic activity up to the easily attainable optimum conditions by slight modification of the surface of graphene via a mild doping process. In order to compare the electrochemical performances of four types of p-doped 3D-GNs and Pt, cyclic voltammetry was carried out in electrolytes of 0.1 M LiClO₄, 10 mM LiI, and 0.5 mM I₂ solutions, as shown in Figure 2c. The relatively negative potential peak between two positive current peaks was assigned to the oxidation reaction $3I^- \rightarrow I_3^- + 2e^-$ and the relatively negative potential peak between two negative current peaks was assigned to the reduction reaction $I_3^- + 2e^- \rightarrow 3I^-$.¹⁶ The oxidation/reduction current density increases with an increase of the catalytic surface area.^{17, 18} The peak-to-peak separation (ΔE_p) for the I₃/I redox reaction decreases with increased feasibility of catalytic reactions.^{11, 14} As shown in Figures 2a and 2c, a negative relationship between the amount of dopants and ΔE_p is observed. Notably, all 3D-GNs exhibit an apparently lower ΔE_p and greater current density compared with the Pt electrode, indicating greater electrochemical catalytic activity and catalytic surface area of 3D-GNs. 3D-GN-5 shows the minimum value of ΔE_p and the maximum value of the current density, which reflect most superior accommodation of large surface area, strong catalytic effect, and high conductivity of optimized 3D-GNs. The excellent catalytic activity of 3D-GNs can be further confirmed by the slope in the Tafel curves,^{19, 20} which represents the relationship between the current density passing through an electrode and the overpotential during oxidation or reduction of the electrode. The Tafel curves of the symmetric dummy cells of 3D-GNs with an apparently greater slope than that of Pt as well as the monotonic relationship between the content of dopants and the logarithmic current density in Figure 2d, clearly present greater electrochemical catalytic activities and diffusion characteristics of (p-doped) 3D-GNs.

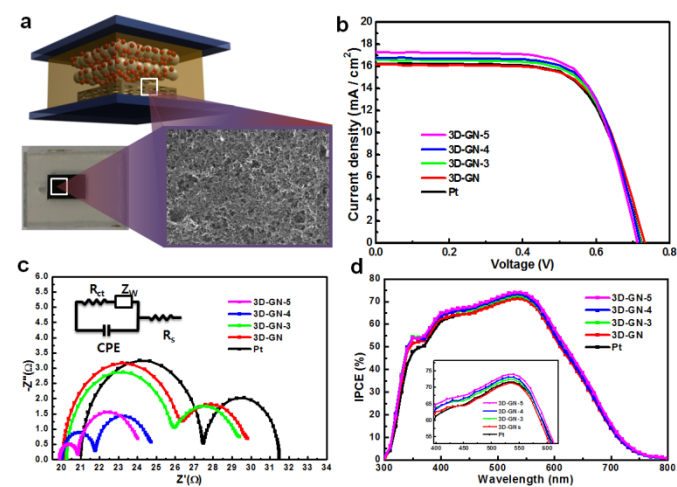


Figure 3. Photovoltaic performance for DSSC using 3D-GN CEs and Pt CE under illumination of AM 1.5. a) Schematic diagram of DSSC with 3D-GN CE. b) I-V curves. c) EIS curves of the symmetric cells. The inset is an equivalent circuit used for fitting the data. d) IPCE spectra of DSSC cells.

In order to exploit the potential application of 3D-GNs as a single component CE in a DSSC device, photovoltaic performance of a DSSC cell fabricated with 3D-GNs was evaluated. Figure 3a displays a schematic illustration of the DSSC cell (top), a photograph of the devices (lower left panel), and a SEM image of the 3D-GN CE (lower right panel). The SEM image confirms the

presence of densely packed and tightly connected 3D graphene networks in the CE. Figure 3b presents the photocurrent-voltage curves of DSSCs with 3D-GN CEs at an illumination intensity of AM 1.5 alongside that of a DSSC with a Pt CE reference cell. The power conversion efficiency of the p-doped 3D-GNs increased with an increase of the content of N and O, showing a maximum value of 8.46% at an optimized condition of 0.5wt% N content with conductivity of 7 S/cm, which is 6.01% higher than that of Pt (7.98%). A relatively greater short circuit current density (J_{sc}) than that of Pt (16.3 mA/cm²) was observed for the 3D-GN based samples, as anticipated from the high surface area of the 3D-GNs (1,025 m²/g). A comparable open circuit voltage (V_{oc}) to that for the Pt CE was observed for the 3D-GN based CEs, reflecting an appropriate band gap difference between the Fermi level of the TiO₂ electrode and the redox potential of I⁻/I₃⁻. Importantly, all the 3D-GN CEs showed greater fill factor (FF) than the Pt CE (67.6%), indicating lower internal resistance in the 3D-GN-based DSSCs. Note that the power conversion efficiency of the pristine 3D-GNs without any doping treatment is already slightly higher than that of Pt (8.11 vs 7.98). The highest value of the O content for the sample having highest conversion efficiency at 0.5wt% N content indicates that the surface of pristine 3D-GNs was further activated by the maximum amount of oxygen for the enhanced catalytic properties and improved conductivity. The effect of doping of pristine 3D-GNs on the performance of DSSCs can be further confirmed by the electrochemical impedance spectroscopy (EIS) data, which show the internal resistance and charge transfer resistance at the interface of the electrodes and the electrolyte for the 3D-GN CEs and Pt CE as shown in Figure 3c. Charge-transfer resistance (R_{ct}) of the electrode surface, which is responsible for the first semicircle (high-frequency region) in the impedance curve, is widely used for evaluating the catalytic activity of CEs. Diffusion of electrolyte species is related to the second semicircle (low frequency region), which is explained by the Nernst diffusion impedance (Z_w). As clearly shown in the impedance curves in Figure 3c (and Table 1), both R_{ct} and the diameter of second semicircles (Z_w) are notably decreased, as the content of both N and O of 3D-GNs is increased. Importantly, a greatly reduced charge transfer resistance (the smaller first circle) between the highly doped 3D-GN CE (3D-GN-4 and 3D-GN-5) and the electrolyte as compared to that between Pt and the electrolyte is observed. 3D-GN-5 with maximum N and O content shows the smallest R_{ct} and Z_w value with the best overall impedance curve, clearly indicating a fast electron transfer mechanism synergistically supported by optimum conductivity and catalytic activity as well as large catalytic surface area. This is in accordance with the data obtained from the CV measurements and Tafel curves in Figures 2c and 2d.

Table 1. Photovoltaic characteristics of DSSC cells with Pt CE and 3D-GN CEs with various contents of N and O.

	R_s (Ω)	R_{ct} (Ω)	Z_w (Ω)	V_{oc} (V)	J_{sc} (mAcm ⁻²)	FF (%)	η (%)
Pt	21.0	7.5	4.0	0.725	16.3	67.6	7.98
3D-GN	20.07	6.1	3.7	0.734	16.2	68.3	8.11
3D-GN-3	20.25	5.6	3.6	0.724	16.5	68.6	8.20
3D-GN-4	20.07	1.8	2.9	0.721	16.8	69.0	8.36
3D-GN-5	19.89	1.0	2.9	0.713	17.2	69.0	8.46

The number of photogenerated electrons per incident photon as a measure of the incident photon-to-electron conversion efficiency (IPCE) was obtained for the conventional Pt CE and 3D-GN CEs, as shown in Figure 3d. The reference Pt CE and 3D-GN-5 exhibit maximum IPCE values of 71.64 % and 73.13% at 540 nm, respectively, thus indicating improved performance of the p-doped

sample that is superior to Pt. Besides, the values on the IPCE curves of the 3D-GN samples with higher O content levels were relatively high and show good agreement with the cell performance data.

In summary, we have developed a straightforward method to achieve mass-producible DSSCs via precursor-assisted CVD grown 3D-GNs with large-surface area and excellent conductivity. DSSCs based on the pristine single component 3D-GNs without any treatment record comparable efficiency to Pt. The efficiency of a DSSC cell fabricated with an optimized p-doped 3D-GN CE is 6.01% superior to the efficiency obtained with a Pt CE cell, which implies the potential of 3D-GNs as an outstanding alternative to Pt. This is very promising considering that the efficiency of 3D-GN based DSSCs could be further enhanced by fine tuning several parameters for device fabrication such as improving adhesion and additional optimization of doping conditions, which is under study. The outstanding performance of 3D-GNs as a CE in DSSCs fabricated with easy and inexpensive method suggests that this straightforward route can be exploited to achieve nano-textured 3D graphene with strong potential for use in other applications as well as for energy-related materials.

Notes and references

Interdisciplinary School of Green Energy and Low Dimensional Carbon Materials Center, UNIST, Korea. E-mail: clau@unist.ac.kr

This work is supported by NRF with the contract no. NRF-2010-0019408 and NRF-2012-R1A1A2043076 and by the development program of local science park funded by the ulsan metropolitan city and the MSIP.

† Electronic Supplementary Information (ESI) available: Experimental details and supplementary figures. See DOI: 10.1039/c000000x/

- B. O'Regan and M. Gratzel, *Nature*, 1991, **353**, 737-740.
- Y. T. Tang, X. Pan, C. N. Zhang, S. Y. Dai, F. T. Kong, L. H. Hu and Y. F. Sui, *J. Phys. Chem. C*, 2010, **114**, 4160-4167.
- Z. Yang, T. Chen, R. He, G. Guan, H. Li, L. Qiu and H. Peng, *Adv. Mater.*, 2011, **23**, 5436-5439.
- Y. H. Xue, J. Liu, H. Chen, R. G. Wang, D. Q. Li, J. Qu and L. M. Dai, *Angew. Chem. Int. Edit.*, 2012, **51**, 12124-12127.
- M. H. Yeh, C. L. Sun, J. S. Su, L. Y. Lin, C. P. Lee, C. Y. Chen, C. G. Wu, R. Vittal and K. C. Ho, *Carbon*, 2012, **50**, 4192-4202.
- H. Bi, F. Q. Huang, J. Liang, X. M. Xie and M. H. Jiang, *Adv. Mater.*, 2011, **23**, 3202-3326.
- A. Reina, X. T. Jia, J. Ho, D. Nezich, H. B. Son, V. Bulovic, M. S. Dresselhaus and J. Kong, *Nano Lett.*, 2009, **9**, 30-35.
- M. D. Stoller, S. J. Park, Y. W. Zhu, J. H. An and R. S. Ruoff, *Nano Lett.*, 2008, **8**, 3498-3502.
- J.-C. Yoon, J.-S. Lee, S.-I. Kim, K.-H. Kim and J.-H. Jang, *Sci. Rep.*, 2013, **3**, 3330.
- Z. Chen, W. Ren, L. Gao, B. Liu, S. Pei and H.-M. Cheng, *Nat Mater*, 2011, **10**, 424-428.
- M. Wu, Q. Zhang, J. Xiao, C. Ma, X. Lin, C. Miao, Y. He, Y. Gao, A. Hagfeldt and T. Ma, *J. Mater. Chem.*, 2011, **21**, 10761-10766.
- K. S. Lee, W. J. Lee, N. G. Park, S. O. Kim and J. H. Park, *Chem. Commun.*, 2011, **47**, 4264-4266.
- L. Kavan, J. H. Yum and M. Gratzel, *ACS Nano*, 2011, **5**, 165-172.
- J. D. Roy-Mayhew, D. J. Bozym, C. Punckt and I. A. Aksay, *ACS Nano*, 2010, **4**, 6203-6211.
- S. Das, P. Sudhagar, E. Ito, D.-y. Lee, S. Nagarajan, S. Y. Lee, Y. S. Kang and W. Choi, *J. Mater. Chem.*, 2012, **22**, 20490-20497.
- A. I. Popov and D. H. Geske, *J. Am. Chem. Soc.*, 1958, **80**, 1340-1352.
- F. Gong, Z. Li, H. Wang and Z.-S. Wang, *J. Mater. Chem.*, 2012, **22**, 17321-17327.
- H. Jeong, Y. Pak, Y. Hwang, H. Song, K. H. Lee, H. C. Ko and G. Y. Jung, *Small*, 2012, **8**, 3757-3761.
- Z. Lan, J. Wu, J. Lin and M. Huang, *J. Mater. Chem.*, 2012, **22**, 3948-3954.
- Z. Tang, Q. Tang, J. Wu, Y. Li, Q. Liu, M. Zheng, Y. Xiao, G. Yue, M. Huang and J. Lin, *RSC Adv.*, 2012, **2**, 5034-5037.